



# An *ab initio* computational study of pure Zn<sub>3</sub>N<sub>2</sub> and its native point defects and dopants Cu, Ag and Au



Nanke Jiang<sup>a</sup>, Jason L. Roehl<sup>b</sup>, Sanjay V. Khare<sup>b,\*</sup>, Daniel G. Georgiev<sup>a</sup>, Ahalapitiya H. Jayatissa<sup>c</sup>

<sup>a</sup> Department of Electrical Engineering and Computer Science, The University of Toledo, 2801 West Bancroft Street, Toledo, OH 43606, USA

<sup>b</sup> Department of Physics and Astronomy, The University of Toledo, Toledo, OH 43606, USA

<sup>c</sup> Department of Mechanical, Industrial, and Manufacturing Engineering, The University of Toledo, Toledo, OH 43606, USA

## ARTICLE INFO

### Article history:

Received 15 October 2013

Received in revised form 15 April 2014

Accepted 14 May 2014

Available online 21 May 2014

### Keywords:

Zinc nitride

First principles

Formation energy

Point defect

Cu family elements

Defect density of states

Bandgap structure

## ABSTRACT

This paper presents the first principles, density functional theory, computations of pure zinc nitride (Zn<sub>3</sub>N<sub>2</sub>) and its doped counterparts with dopants of native elements (Zn, N) and copper family elements (Cu, Ag, Au). Atomic geometry, formation energy, and electronic structure of defects in Zn<sub>3</sub>N<sub>2</sub> are also investigated. The formation energies of both native defects and copper family element impurities are predominantly affected by the chemical potential of different chemical species. The earlier experimental observation of electronic properties associated with nitrogen deficiency in Zn<sub>3</sub>N<sub>2</sub> is consistent with the results of formation energy calculations. Point defects of copper family elements have an energetic preference to occupy a substitutional N site, rather than Zn or interstitial position at a special value of chemical potential of nitrogen. The calculation of defect density of states suggests that among all three copper family elements, copper is the most suitable candidate as a p-type dopant in Zn<sub>3</sub>N<sub>2</sub>.

© 2014 Elsevier B.V. All rights reserved.

## 1. Introduction

Zinc nitride (Zn<sub>3</sub>N<sub>2</sub>) is a II–V compound semiconductor [1], which is considered as a promising material, for electronic, optoelectronic, photovoltaic and sensor applications because of its favorable optical and electrical properties [2–4]. It offers additional advantages such as environmentally-friendly processing, non-toxicity, earth abundance of zinc, and potentially low fabrication cost [5–7]. Although first synthesized more than 70 years ago [8], zinc nitride remains relatively unexplored and its physical properties are not well understood. In the last couple of decades, there has been an increase in experimental studies on zinc nitride. Beginning with its structure identification in 1997 [9], zinc nitride has been prepared and studied by various fabrication methods and characterization techniques [1–3,6,10–14]. Theoretical investigation has been restricted to the study of native and oxygen defects [15–17]. Zinc nitride usually exhibits n-type conductivity, which has been confirmed by different experimental groups [6,10–14]. Studies on other physical properties, such as electronic band gap, as well as the transition type (direct or indirect), electronic mobility, and conductivity, have produced data with a large variation [1,3,5,6,10,11,18,19].

In order to apply this material in electronics and photovoltaics, p-type doping of zinc nitride is very important. One possibility is to

create p-type Zn<sub>3</sub>N<sub>2</sub> by doping it with appropriate elements. Copper family elements were investigated as p-type dopants in ZnO [20]. Therefore, our group in University of Toledo is conducting experimental work to study the possibility of copper family elements as p-type dopants for Zn<sub>3</sub>N<sub>2</sub>. However, there has been no theoretical study, in the past, on the effect of possible p-type dopants in zinc nitride. Such an investigation would be intrinsically important and also serve as a guide for future experimental work. Thus, this investigation is focused on the first principles computational exploration of structural, electronic and energetic properties of: (i) pure Zn<sub>3</sub>N<sub>2</sub> and (ii) point defects in Zn<sub>3</sub>N<sub>2</sub> of native elements Zn and N along with those of the copper family namely, Cu, Ag and Au. The band structure of pure Zn<sub>3</sub>N<sub>2</sub> and the electronic structure of pure and defective Zn<sub>3</sub>N<sub>2</sub> were determined. The formation energies of several native defects, as well as those of the copper family, were computed. Our results indicate that Zn<sub>3</sub>N<sub>2</sub> is a small bandgap material with a direct band transition behavior. We observe that the formation energies of both native defects and copper family element impurities are affected dramatically by the chemical potential of different atomic species. At a special value of chemical potential of nitrogen, copper family elements energetically favor occupancy of a nitrogen substitutional site, rather than a zinc or interstitial position. However, the three elements of the copper family show differences in individual electronic character while occupying a nitrogen site. The electronic structure of Cu-doped Zn<sub>3</sub>N<sub>2</sub> supports strong p-type behavior whereas doping of Ag or Au did not show such an effect.

\* Corresponding author. Tel.: +1 419 530 2292; fax: +1 419 530 2723.  
E-mail address: [sanjay.khare@utoledo.edu](mailto:sanjay.khare@utoledo.edu) (S.V. Khare).

## 2. Computational method

All computations were performed by *ab initio* total energy calculations within the generalized gradient (GGA) and local density (LDA) approximations to density-functional theory [21,22] using the Vienna *ab initio* simulation package [23–26] of codes. In this implementation, core electrons are implicitly treated by ultrasoft Vanderbilt type pseudopotentials [27] as supplied by Kresse et al. [28] using the Ceperly and Alder exchange-correlation functional as parameterized by Perdew and Zunger for the LDA [29] and by Perdew and Wang (PW91) for the GGA [30,31]. For each calculation, irreducible  $k$ -points were generated according to the Monkhorst–Pack scheme [32]. A  $k$ -point density equivalent to 4  $k$ -points in the irreducible part of the Brillouin zone resulted from tests for energy convergence in the 40-atom primitive cell. The single-particle wave functions were expanded in a plane-wave basis using a 420 eV energy cutoff for LDA and 460 eV for GGA. These values were determined to be sufficient by performing convergence tests for an accuracy of 1 meV. The absolute minimum in total energy was obtained by varying the lattice constant. Full relaxation of ions was performed to find the minimum energy for each configuration. All atoms were allowed to relax until a force tolerance of 1 meV/Å was reached for each atom. The calculations for the density of states (DOS) and local density of states (LDOS) were performed with Methfessel–Paxton scheme for the energy [33]. Computations for inclusion of defects were performed in a supercell with 320 atoms of pure  $\text{Zn}_3\text{N}_2$  constructed by periodically repeating the 40-atom primitive cell in three dimensions. Based on the type of defects, an atom of a different kind was either added or removed or replaced in these supercells of  $\text{Zn}_3\text{N}_2$ .

## 3. Results and discussion

### 3.1. Optimized structure of pure zinc nitride

Pure zinc nitride belongs to the space group  $Ia\bar{3}$  with space group number 206. It has a cubic anti-bixbyite structure with a Pearson symbol cI80 [9]. The primitive cell of  $\text{Zn}_3\text{N}_2$  consists of a  $\text{Zn}_{24}\text{N}_{16}$  unit of 40 atoms in a cubic shape. We computed the lattice constant of this cell to be 9.839 Å by using GGA as shown in Table 1 or 9.601 Å by using LDA. Based on the percent error, which is within 0.7% by GGA or 1.7% by LDA when comparing with the established value, 9.77 Å [9], GGA was selected for all computations that follow. Positions of the forty atom basis in this cell are obtained from International Tables for Crystallography [34] and the corresponding atomic structure is shown in Fig. 1. The  $\text{Zn}_3\text{N}_2$  structure can be regarded as a face-centered cubic (fcc) arrangement of N atoms with the larger Zn atoms occupying 3/4 of the tetrahedral sites. The absence of the Zn atoms in the unoccupied tetrahedral holes produces a slight distortion of the fcc structure, as shown in Fig. 1. The N atoms forming the fcc lattice occupy two distinct N positions. The first type of position, N1, is the  $8b$  Wyckoff position [34] while the second type, N2, is the  $24d$  Wyckoff position. The Zn atoms in the tetrahedral sites occupy the  $48e$  Wyckoff position. As a result of the

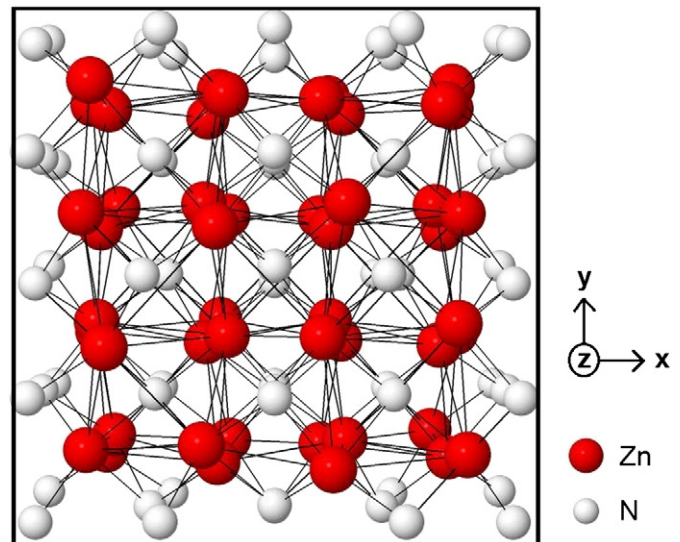


Fig. 1. Atomic structure of pure  $\text{Zn}_3\text{N}_2$  (along  $z$  direction); red (larger) circles represent zinc atoms, and white (smaller) circles represent nitrogen atoms. Shown is an 80 atom unit cell.

distortion, the Zn atoms in the tetrahedral sites have three distinct nearest-neighbor Zn–N2 distances. More details about atomic geometry are described in next section. The bulk modulus was computed to be 140.2 GPa with GGA and 176.6 GPa with LDA. A comparison with other published values is shown in Table 1.

We show the computed band structure of pure zinc nitride in Fig. 2, along with the electronic DOS. Fig. 2 shows that the conduction band (CB) minimum and the valence band (VB) maximum are both located at the  $\Gamma$  point. The band structure also shows no band gap due to the well-known error in the LDA and GGA methods of density functional theory, which leads to the underestimation of approximately 50% or more in many nitrides [35]. Differences in fabrication methods are known to cause significant changes in physical properties of this material. A common contaminant, upon growth of zinc nitride films, is oxygen of which there is always a small fraction estimated to be at least about 5% in the material and which occurs in many other nitrides [6,36]. In general, larger fraction of oxygen contained in film will result in the increase of the band gap value, up to the value of ZnO, 3.2 eV. Thus there is a large uncertainty in the experimental values for the band gap in the literature with reported values of 1.26 eV [6], 2.25 eV [37] and 3.2 eV [1]. This large uncertainty precludes the fixing of the band gap with the LDA + U technique applicable in other materials such as Si or GaAs where the band gap is precisely known experimentally.

The DOS in Fig. 2 indicates that the states near the top of the VB arise mainly from N-2p states and Zn-3d states. The peak in the CB at around 2 eV is dominated by N-2p, Zn-4s and Zn-3p states. This observation is

**Table 1**  
Calculated and experimental structural data, lattice constant  $a$ , bulk modulus  $B$ , bond lengths between the Zn atom and nearest N atom of the first or second type  $d_{(\text{Zn}-\text{N}1)}$  and  $d_{(\text{Zn}-\text{N}2)}$  respectively, in the  $\text{Zn}_3\text{N}_2$  structure.

Structure	This work	Other theoretical results	Other experimental results
$a$ (Å)	9.839 (GGA)	9.667 <sup>a</sup> , 9.769 <sup>b</sup>	9.7691 (1) <sup>c</sup> , 9.758 <sup>d</sup>
$d_{(\text{Zn}-\text{N}1)}$ (Å)	2.14 (GGA)	2.095 <sup>a</sup> , 2.122 <sup>b</sup>	2.133 <sup>c</sup>
$d_{(\text{Zn}-\text{N}2)}$ (Å)	2.01, 2.06, 2.33 (GGA)	(1.990, 2.019, 2.096) <sup>a</sup> (2.002, 2.060, 2.287) <sup>b</sup>	(1.996, 2.068, 2.262) <sup>c</sup>
$B$ (GPa)	140.2 (GGA) 176.6 (LDA)	202.2 <sup>a</sup>	228(2) <sup>e</sup>

<sup>a</sup> Ref. [17], theory uses GGA.

<sup>b</sup> Refs. [15,16], theory uses LDA.

<sup>c</sup> Ref. [9], experiment.

<sup>d</sup> Ref. [6], experiment.

<sup>e</sup> Ref. [35], experiment.

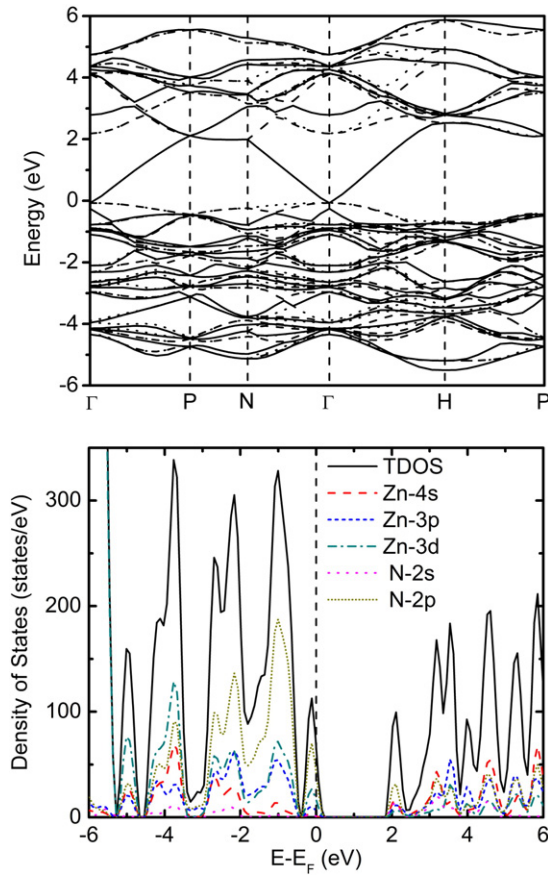


**Fig. 2.** Band structure and density of states (DOS) of pure Zn<sub>3</sub>N<sub>2</sub>. The Fermi energy ( $E_F$ ) is set to zero and represented by the dashed line.

consistent with previous theoretical work on zinc nitride [16,17]. The appearance of N-2p states, near the Fermi energy, in the VB and CB signifies their importance in the electronic behavior of zinc nitride.

### 3.2. Atomic geometry of pure and defective Zn<sub>3</sub>N<sub>2</sub>

The bond lengths in pure Zn<sub>3</sub>N<sub>2</sub> are 2.14 Å for Zn–N1 and 2.01 Å, 2.06 Å, and 2.33 Å for Zn–N2. These values listed in Table 1 are in agreement with previous theoretical [15–17] and experimental work [6,9,38]. The geometry of atomic positions was influenced by the type of defect introduced. When a vacancy was formed at the N1 position, the nearest Zn neighbors, six in total, were pushed farther apart by ~8%. However, in the cases of vacancies at N2 or Zn positions, nearest neighbors, six Zn atoms or four N atoms respectively, remained almost unchanged. Their mutual distances changed by less than 0.5%. It shows that the effect of the relaxation response by introducing an N vacancy is strongly influenced by its location and nearest neighbor environment. For an interstitial defect (D) introduced at the high symmetry Wyckoff position 8a, (0, 0, 0), there are six Zn and six N nearest neighbor atoms. The average bond lengths from D to Zn atoms and D to N atoms are,

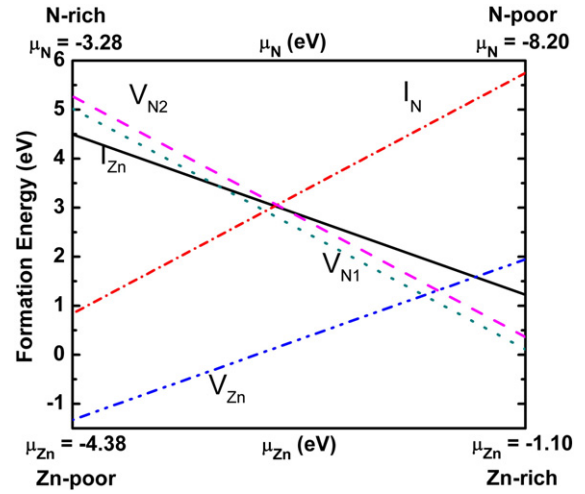


**Fig. 3.** Native defect formation energies for (i) a vacancy at the first type of nitrogen site ( $V_{N1}$ ), (ii) a vacancy at the second type of nitrogen site ( $V_{N2}$ ), (iii) a vacancy at the zinc site ( $V_{Zn}$ ), (iv) a nitrogen interstitial ( $I_N$ ), and (v) a zinc interstitial ( $I_{Zn}$ ) as a function of chemical potential of single N atom, top axis and Zn atom, bottom axis. Both interstitials are positioned at high symmetry Wyckoff position 8a (0, 0, 0).

respectively, 2.48 Å and 2.38 Å (for D = Zn), 2.15 Å and 2.65 Å (for D = N), 2.41 Å and 2.46 Å (for D = Cu), 2.50 Å and 2.56 Å (for D = Ag), and 2.52 Å and 2.60 Å (for D = Au). Similarly when copper family elements substituted N at the N1 position, the average bond lengths to nearest Zn atoms were 2.48 Å (for Cu) and 2.59 Å (for Ag and Au), all of which are larger than the one in pure Zn<sub>3</sub>N<sub>2</sub>, of 2.14 Å. These changes in the bond lengths suggest that radii of the defect atoms are the main factor determining the atomic geometry for this interstitial position. This contrasts with the case when copper family elements substituted Zn. Then the bond lengths to N at N1 position are 2.14 Å (for Cu), 2.46 Å (for Ag) and 2.33 Å (for Au). All these values are closer to the value in pure Zn<sub>3</sub>N<sub>2</sub> of 2.14 Å. These lengths cannot be explained away merely by the differing atomic radii. The electronic bonding differences affect these lengths. The same trend is observed for bond lengths from the defect atom to N at the N2 site.

### 3.3. Defect formation energies

#### 3.3.1. Formation energy calculation

Following standard practice [39–44] we computed the defect (D) formation energies,  $E_{form}(D, q)$ , in charge state  $q$ , by the equation:

$$E_{form}(D, q) = E_{def}(D, q) - E_{pure}(Zn_3N_2) - n_{Zn}\mu_{Zn} - n_N\mu_N - n_D\mu_D + q(\mu_e + E_v) \quad (1)$$

where  $n_i$  ( $i = Zn, N$  or  $D$ ) denotes the number of atoms of type  $i$  that were added to ( $n_i = +1$ ) and/or removed from ( $n_i = -1$ ) the supercell when the defect was introduced with  $\mu_i$  being the corresponding chemical potential of the species  $i$  [40,45]. The electron chemical potential is  $\mu_e$  [46] and the valence band maximum in the pure supercell, with no defect, is  $E_v$ . The energy  $E_{def}(D, q)$  is computed for a supercell containing the relaxed defect D in charge state  $q$  and

**Table 2**  
The energy of formation of zinc nitride (Zn<sub>3</sub>N<sub>2</sub>) and related nitrides.

Type of nitrides	Energy of formation (eV)	
	$\mu_N = -8.26$ eV Half of the total energy of the N <sub>2</sub> molecule	$\mu_N = -3.28$ eV Total energy of a single spin-polarized N atom
Zn <sub>3</sub> N <sub>2</sub>	0.13	−9.83
Cu <sub>3</sub> N	1.21	−8.75
Ag <sub>3</sub> N	2.57	−7.39
AuN	3.26	−6.70

**Table 3**  
Formation energies (in eV) of native defects of Zn<sub>3</sub>N<sub>2</sub>.

Types of defects	$E_{\text{form}}$ (eV)	
	N-poor condition ( $\mu_{\text{N}} = -8.20$ eV; $\mu_{\text{Zn}} = -1.10$ eV)	N-rich condition ( $\mu_{\text{N}} = -3.28$ eV; $\mu_{\text{Zn}} = -4.38$ eV)
$I_{\text{Zn}}$	1.22	4.50
$I_{\text{N}}$	5.76	0.84
$V_{\text{Zn}}$	1.95	-1.33
$V_{\text{N1}}$	0.11	5.02
$V_{\text{N2}}$	0.36	5.27

$E_{\text{pure}}(\text{Zn}_3\text{N}_2)$  is the total energy of a supercell of the same size with no defect. Considering several charge states is beyond the scope of the size of the current article. Hence, we will focus on the defects in neutral state ( $q = 0$ ). Therefore, Eq. (1) simplifies to:

$$E_{\text{form}}(\text{D}, 0) = E_{\text{def}}(\text{D}, 0) - E_{\text{pure}}(\text{Zn}_3\text{N}_2) - n_{\text{Zn}}\mu_{\text{Zn}} - n_{\text{N}}\mu_{\text{N}} - n_{\text{D}}\mu_{\text{D}} \quad (2)$$

It is difficult to determine the values of  $\mu$  for different species in a given experimental setup purely from *ab initio* methods. Even so, under equilibrium growth conditions, there are some thermodynamic limits on the chemical potentials  $\mu_i$  which we now list. First, to avoid precipitation, the chemical potentials of Zn, N, and/or the impurity D ( $\text{D} = \text{Cu}, \text{Ag}, \text{Au}$ ) are bound by the conditions:

$$\mu_{\text{Zn}} \leq \mu_{\text{Zn,bulk}}, \quad \mu_{\text{N}} \leq \mu_{\text{N,Max}}, \quad \mu_{\text{D}} \leq \mu_{\text{D,bulk}}, \quad (3)$$

where  $\mu_{\text{Zn,bulk}}$  is the total energy per Zn atom, computed in the bulk hexagonal closed pack phase of metal Zn, and  $\mu_{\text{D,bulk}}$  was computed from fcc bulk phases of Cu, Ag and Au. Depending on fabrication conditions,  $\mu_{\text{N,Max}}$  is the maximum possible chemical potential of the nitrogen atom, which is discussed in Section 3.3.2.

Second,  $\mu_i$  is limited to those values that maintain a stable Zn<sub>3</sub>N<sub>2</sub> compound, and therefore is bound by

$$3\mu_{\text{Zn}} + 2\mu_{\text{N}} = \mu_{\text{pure}}(\text{Zn}_3\text{N}_2) \quad (4)$$

where  $\mu_{\text{pure}}(\text{Zn}_3\text{N}_2)$  is the energy per formula unit Zn<sub>3</sub>N<sub>2</sub>. Combining results from Eqs. (3) and (4) we obtain the limits:

$$\left(\mu_{\text{pure}}(\text{Zn}_3\text{N}_2) - 2\mu_{\text{N,Max}}\right) / 3 \leq \mu_{\text{Zn}} \leq \mu_{\text{Zn,bulk}} \quad (5)$$

and

$$\left(\mu_{\text{pure}}(\text{Zn}_3\text{N}_2) - 3\mu_{\text{Zn,bulk}}\right) / 2 \leq \mu_{\text{N}} \leq \mu_{\text{N,Max}}. \quad (6)$$

**Table 4**  
Computed formation energies (in eV) of single atom Cu, Ag and Au defects as interstitials or substitution defects in Zn<sub>3</sub>N<sub>2</sub>.

Types of defects	$E_{\text{form}}$ (eV)	
	N-poor condition ( $\mu_{\text{N}} = -8.20$ eV; $\mu_{\text{Zn}} = -1.10$ eV)	N-rich condition ( $\mu_{\text{N}} = -3.28$ eV; $\mu_{\text{Zn}} = -4.38$ eV)
$\text{Cu}_{\text{Zn}}$	1.57	-0.45
$\text{Ag}_{\text{Zn}}$	2.44	-0.04
$\text{Au}_{\text{Zn}}$	2.98	1.42
$\text{Cu}_{\text{N1}}$	9.65	5.51
$\text{Ag}_{\text{N1}}$	9.43	5.54
$\text{Au}_{\text{N1}}$	8.87	4.64
$\text{Cu}_{\text{N2}}$	10.39	6.25
$\text{Ag}_{\text{N2}}$	10.39	6.50
$\text{Au}_{\text{N2}}$	9.82	5.59
$I_{\text{Cu}}$	2.19	2.19
$I_{\text{Ag}}$	3.18	3.18
$I_{\text{Au}}$	4.00	4.00

Finally, to avoid the formation of secondary phases between the impurity D and the host elements,  $\mu_i$  is limited by

$$a\mu_{\text{D}} + b\mu_{\text{Zn}} < E_{\text{pure}}(\text{D}_a\text{Zn}_b), \quad (7)$$

for substitution defects at N sites and

$$a\mu_{\text{D}} + b\mu_{\text{N}} < E_{\text{pure}}(\text{D}_a\text{N}_b), \quad (8)$$

for substitution defects at Zn sites. Here  $a$  and  $b$  are the number of impurity D and host atoms in the formula unit of the respective stable alloy ( $\text{D}_a\text{Zn}_b$ ) or nitride ( $\text{D}_a\text{N}_b$ ) phases. The energy  $E_{\text{pure}}(\text{D}_a\text{Zn}_b)$  is the total energy of the alloy  $\text{D}_a\text{Zn}_b$ , and  $E_{\text{pure}}(\text{D}_a\text{N}_b)$  presents the total energy of  $\text{Cu}_3\text{N}$ ,  $\text{Ag}_3\text{N}$  or  $\text{AuN}$  computed from their most stable cubic phases which belong to space group of  $\text{Pm}\bar{3}\text{m}$ ,  $\text{Pm}\bar{3}\text{m}$ ,  $\text{Fm}\bar{3}\text{m}$ , respectively. For small concentrations (<1%) of either Cu or Ag or Au added as dopants, the corresponding alloy phase diagrams [47–49] show alloys in the hexagonal close pack phase. Therefore we computed  $E_{\text{pure}}(\text{D}_a\text{Zn}_b)$  values with a large supercell of 1 D ( $\text{D} = \text{Cu}, \text{Ag}, \text{Au}$ ) atom and 127 Zn atoms. For substitution defects at Zn sites Eqs. (3) and (8) give two different limits for the upper bound on  $\mu_{\text{D}}$ . We need to choose the minimum of these two limits. A similar case occurs for the substitution defects at N sites with Eqs. (3) and (7). We then get the final limits:

$$\mu_{\text{D,Max}} = \min\left(\mu_{\text{D,bulk}}, \left(E_{\text{pure}}(\text{D}_a\text{Zn}_b) - b\mu_{\text{Zn}}\right) / a\right) \text{ for } D_{\text{N1}} \text{ and } D_{\text{N2}} \quad (9)$$

and

$$\mu_{\text{D,Max}} = \min\left(\mu_{\text{D,bulk}}, \left(E_{\text{pure}}(\text{D}_a\text{N}_b) - b\mu_{\text{N}}\right) / a\right) \text{ for } D_{\text{Zn}}. \quad (10)$$

### 3.3.2. Chemical potential of nitrogen

As mentioned in the previous section,  $\mu_{\text{N}}$  is important for the defect formation energy computations, and its maximum,  $\mu_{\text{N,Max}}$ , will affect the computation results significantly. In general,  $\mu_{\text{N,Max}}$  is computed as half

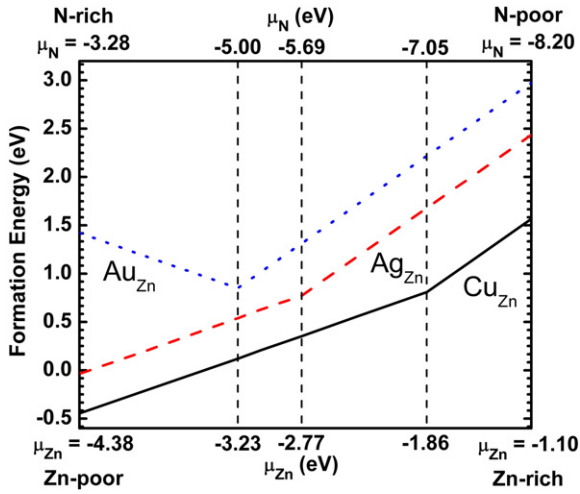


Fig. 4. Formation energies for different substitution defects,  $\text{Cu}_{\text{Zn}}$ ,  $\text{Ag}_{\text{Zn}}$  and  $\text{Au}_{\text{Zn}}$ , at Zn position as a function of chemical potential of single N atom. Dashed lines signify values of  $\mu_{\text{Zn}}$  and  $\mu_{\text{N}}$  where there is a change in slope of the formation energy lines.

of the total energy of the  $\text{N}_2$  molecule [43,50,51]. However, the nitrides of transition metals,  $\text{X}_a\text{N}_b$ , especially of copper family elements, are extremely difficult to form. Their energy of formation is calculated as:

$$E_f(\text{X}_a\text{N}_b) = \mu(\text{X}_a\text{N}_b) - a\mu_{\text{X}} - b\mu_{\text{N}}, \quad (11)$$

where  $\mu(\text{X}_a\text{N}_b)$  is the energy per formula unit  $\text{X}_a\text{N}_b$  ( $\text{X} = \text{Zn}, \text{Cu}, \text{Ag}, \text{or Au}$ ), and  $a$  and  $b$  are the number of element X and nitrogen in their stable nitride ( $\text{X}_a\text{N}_b$ ) phases. Table 2 shows the positive energy of formation of  $\text{X}_a\text{N}_b$  (namely,  $\text{Zn}_3\text{N}_2$ ,  $\text{Cu}_3\text{N}$ ,  $\text{Ag}_3\text{N}$  and  $\text{AuN}$ ) calculated by using  $\mu_{\text{N}}$  as half of the total energy of the  $\text{N}_2$  molecule, verifying this observation as well. This problem is caused because molecular nitrogen  $\text{N}_2$ , when directly used as a nitrogen source in growth, cannot form the metal–nitrogen bond. It needs to transform to a charged species such as  $\text{N}^{3-}$  [35,52–55]. In order to overcome this problem, extra energy should be provided to help the charge separation by increasing the  $\mu_{\text{N}}$  via use of intermediate compounds or plasma source or both [39,56,57]. Therefore, we have used, as  $\mu_{\text{N,Max}}$ , the chemical potential value, of  $-3.28$  eV, of a

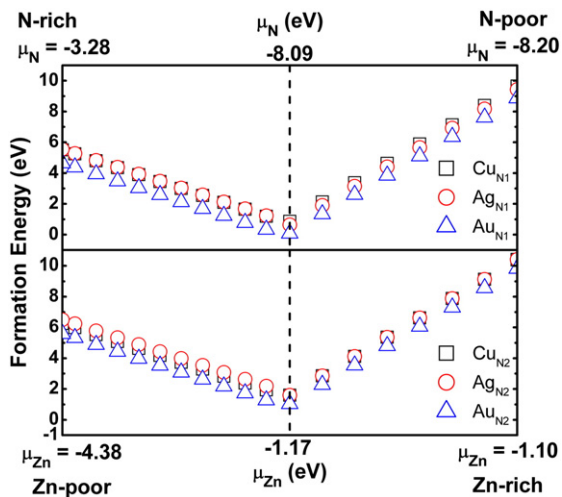


Fig. 5. Formation energies for different substitution defects at N1 and N2 position of nitrogen as a function of chemical potential of single N atom. Note that the X axis is not uniform with break in uniformity shown by the dashed line. The breaks also signify values of  $\mu$  where there is a change in slope of the formation energy lines.

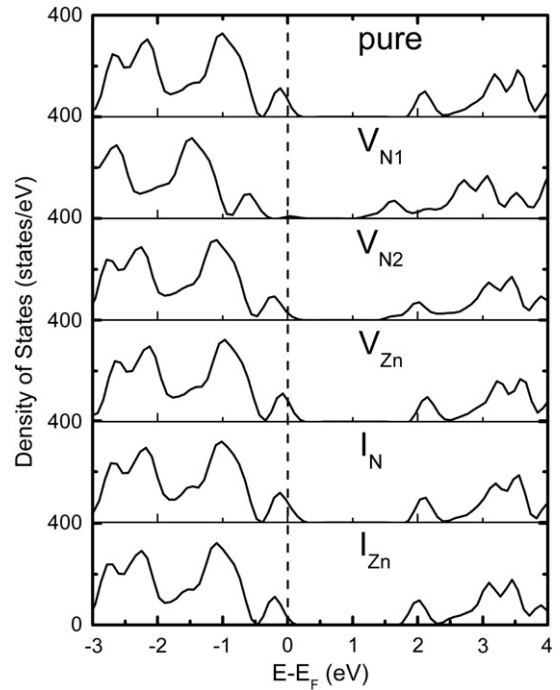


Fig. 6. DOS of  $\text{Zn}_3\text{N}_2$  (pure) with no defects and with different types of native defects: a vacancy at the first type of nitrogen site ( $\text{V}_{\text{N1}}$ ), a vacancy at the second type of nitrogen site ( $\text{V}_{\text{N2}}$ ), a vacancy at the zinc site ( $\text{V}_{\text{Zn}}$ ), a nitrogen interstitial ( $\text{I}_{\text{N}}$ ), and a zinc interstitial ( $\text{I}_{\text{Zn}}$ ). Both interstitials are positioned at high symmetry Wyckoff position 8a (0, 0, 0). Energy is relative to the Fermi energy ( $E_{\text{F}}$ ) represented by the dashed line.

spin-polarized single N atom instead of half the total energy of the  $\text{N}_2$  molecule,  $-8.26$  eV. This value accounts for the breakup of the  $\text{N}_2$  molecule which occurs during growth due to the plasma and the resulting complex chemical alteration of the  $\text{N}_2$  molecule. From this changed

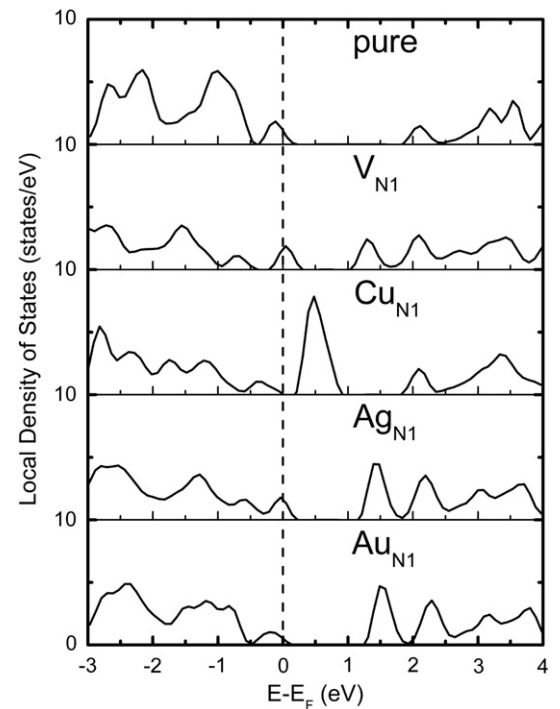
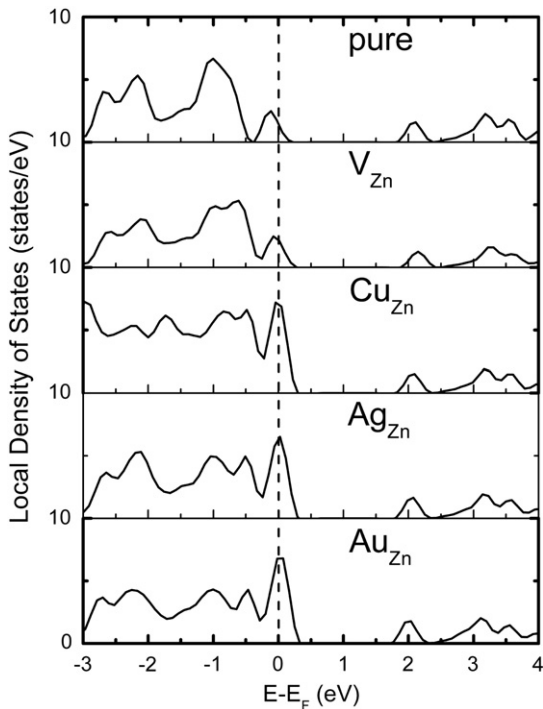


Fig. 7. LDOS of pure  $\text{Zn}_3\text{N}_2$  and with different substitution defects at the N1 position of nitrogen. The LDOS is only the portion of total density of states projected onto the defect and its nearest neighbor atoms. Energy is relative to the Fermi energy ( $E_{\text{F}}$ ) represented by the dashed line.



**Fig. 8.** LDOS of pure  $\text{Zn}_3\text{N}_2$  and with different substitution defects at the Zn position. The LDOS is only the portion of total density of states projected onto the defect and its nearest neighbor atoms. Energy is relative to the Fermi energy ( $E_F$ ) represented by the dashed line.

value of  $\mu_N$  emerges the, physically more meaningful, negative energy of formation of  $\text{X}_a\text{N}_b$  shown in Table 2.

### 3.3.3. Formation energy of native defects

We simulated several possible native defects, namely N vacancy at two types of nitrogen sites ( $V_{N1}$ ,  $V_{N2}$ ), Zn vacancy ( $V_{Zn}$ ), and self-

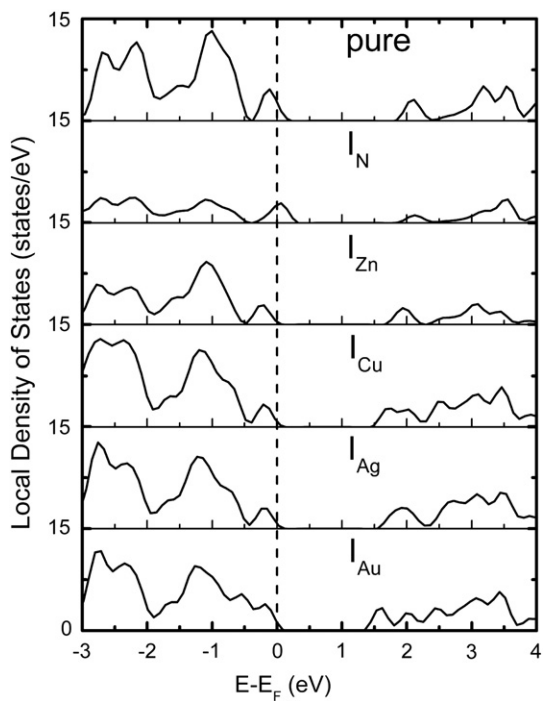


**Fig. 9.** LDOS of pure  $\text{Zn}_3\text{N}_2$  and with different interstitial defects at the Zn position. The LDOS is only the portion of total density of states projected onto the defect and its nearest neighbor atoms. Energy is relative to the Fermi energy ( $E_F$ ) represented by the dashed line.

interstitial of N ( $I_N$ ) and Zn ( $I_{Zn}$ ) at the high symmetry Wyckoff position  $8a$ , (0, 0, 0).

The formation energies for various native defects, computed from Eq. (2) with chemical potential limits deduced from Eqs. (5) and (6), are presented in Fig. 3. Table 3 lists the formation energies for various native defects in two extreme conditions: (i) N-poor (Zn-rich) condition where  $\mu_{Zn}$  reaches its maximum  $\mu_{Zn, \text{bulk}}$  which takes a value of  $-1.10$  eV, and (ii) N-rich (Zn-poor) condition where  $\mu_{Zn}$  reaches its minimum, at  $-4.38$  eV. Due to the limits in Eq. (4), for the first case  $\mu_N$  reaches its minimum at  $-8.20$  eV and in the second case it reaches its maximum at  $-3.28$  eV.

As shown in Table 3 as well as the right-end of Fig. 3, in N-poor (Zn-rich) condition, the small formation energy for an N1 and N2 vacancy, by one order of magnitude compared to other three types of defects ( $V_{Zn}$ ,  $I_{Zn}$ , and  $I_N$ ), may suggest its propensity in experimental observation [3,6,11,18,58,59]. Upon the existence of such vacancies and exposure to air, replacement of N1 site vacancies by oxygen may be possible. The DOS in Fig. 2 has already indicated that nitrogen p states influence the electronic behavior of zinc nitride significantly. Thus differences in N vacancy concentrations may be the reason of disagreement in electronic band gaps reported in experimental work [1,6,37], which differ in sample preparation and hence material chemical composition. In the N-poor condition, next to  $V_{N1}$  and  $V_{N2}$ ,  $I_{Zn}$  has the third lowest formation energy with a value that is only about half of the value of  $V_{Zn}$  and one fifth of the value of  $I_N$ . Based on the observations in earlier experimental work [3,6,11,18,58,59], there is a gradually emerging consensus that excess of zinc and deficiency of nitrogen are the two main factors responsible for n-type conductivity of zinc nitride. Present results here support this conclusion.

With the increase of  $\mu_N$  and simultaneous decrease of  $\mu_{Zn}$ , as depicted in Fig. 3, the formation energies for  $V_{N1}$ ,  $V_{N2}$  and  $I_{Zn}$  increase while those of  $I_N$  and  $V_{Zn}$  decrease. When an N-rich (Zn-poor) condition is reached, the  $V_{Zn}$  will be extremely easy to form while probability of  $I_N$  formation will also be non-trivial, based on the results of formation energy, seen in Table 3 and the left-end of Fig. 3. The presence of these two types of defects will result in p-type conductivity. This observation suggests that by adjusting the chemical potential of nitrogen in the fabrication process, the type of conductivity of the defective zinc nitride can be changed. This may unveil the reason for the different types of electrical conductivity of zinc nitride in previous experimental work, since variations in growth conditions lead to different values of  $\mu_{Zn}$  and  $\mu_N$  affecting defect concentrations significantly [3,5,6,11,18,19,58,59].

### 3.3.4. Formation energy of impurities – Cu family elements

Systematic approaches to synthesize p-doped  $\text{Zn}_3\text{N}_2$  are currently of experimental interest. The copper family elements, Cu, Ag, and Au have one less outer shell electron than zinc. They have also been theoretically investigated earlier, as p-type dopants in zinc oxide [20]. Therefore, the single atom defects of Cu, Ag, and Au are identified as the potential p-type dopants in  $\text{Zn}_3\text{N}_2$ .

The formation energies of zinc nitride with single atom Cu-family element, as an uncharged defect at various positions, were computed from Eq. (2) with chemical potential limits deduced from Eqs. (5), (6), (9), and (10). These positions include the interstitial ( $I_D$ ) at high symmetry Wyckoff position  $8a$  (0, 0, 0) and substitution defects at Zn ( $D_{Zn}$ ), and at two types N sites ( $D_{N1}$  and  $D_{N2}$ ) where,  $D = \text{Cu, Ag, and Au}$ . Table 4 lists the formation energies for these defects in two extreme conditions, (i) N-poor (Zn-rich) condition where  $\mu_{Zn}$  reaches its maximum value,  $\mu_{Zn, \text{bulk}}$ , which equals  $-1.10$  eV and (ii) N-rich (Zn-poor) condition where  $\mu_N$  reaches its maximum value of  $-3.28$  eV.

In Fig. 4, the influence of chemical potential of single N atom on formation energies of substitution defects at Zn position is shown. In N-poor condition (right-end of the figure), the highest possible

chemical potential of defect elements,  $\mu_{D,Max}$ , was found to be  $\mu_{D,bulk}$  from Eq. (10). Therefore, based on Eq. (2) along with Eqs. (4) and (10), the defect formation energy of substitution defects at Zn position was calculated as:

$$E_{form}(D, 0) = E_{def}(D, 0) - E_{pure}(Zn_3N_2) - (-1) \times \left[ (\mu_{pure}(Zn_3N_2) - 2\mu_N) / 3 \right] - (+1) \times \mu_{D,Max}. \quad (12)$$

We note that Eq. (10) indicates that  $\mu_{D,Max} = \mu_{D,bulk}$  when  $\mu_N$  is below a critical value  $\mu_c$ . The value of  $\mu_c$  changes with the defect D and is  $-7.05$  eV for Cu,  $-5.69$  eV for Ag and  $-5.00$  eV for Au. Similarly,  $\mu_{D,bulk}$  is  $-3.77$  eV for Cu,  $-2.72$  eV for Ag, and  $-3.19$  eV for Au. On the other hand if  $\mu_N > \mu_c$  then  $\mu_{D,Max} = (E_{pure}(D_aN_b) - b\mu_N) / a$ . In this latter case  $\mu_{D,Max}$  becomes a function of  $\mu_N$ , instead of being a constant value  $\mu_{D,bulk}$ . This change in the value of  $\mu_{D,Max}$  indicates the shift in propensity for the defects to form bulk precipitates compared to the formation of secondary defect element nitrides. Based on Eq. (12), the defect formation energies for  $Cu_{Zn}$  and  $Ag_{Zn}$  keep decreasing with increasing  $\mu_N$  but with a slow rate of decrease and reach the minima at the N-rich (left-end of the figure) condition, while for  $Au_{Zn}$ , the formation energy increases instead of decreasing with the increase of the  $\mu_N$ . Moreover, as seen in Table 4, formation energies of  $D_{Zn}$  increase with atom radius, of the defect, under N-poor and N-rich conditions.

The defect formation energy of substitution defects at N positions can be written in a similar manner to Eq. (12) as:

$$E_{form}(D, 0) = E_{def}(D, 0) - E_{pure}(Zn_3N_2) - (-1) \times \left[ (\mu_{pure}(Zn_3N_2) - 3\mu_N) / 2 \right] - (+1) \times \mu_{D,Max}. \quad (13)$$

Fig. 5 shows the influence of chemical potential of a single N atom,  $\mu_N$ , on formation energies of substitution defects at N positions, N1 and N2. The change of slope of formation energies is also observed, and it is caused by the similar changes in  $\mu_{D,Max}$ . When  $\mu_N < -8.09$  eV for all three defect elements, including the N-poor condition, the value of  $\mu_{D,Max} = (E_{pure}(D_aN_b) - b\mu_N) / a$ , is a function of  $\mu_N$ . While  $\mu_N$  increases and gets larger than  $-8.09$  eV,  $\mu_D$  takes the constant value of  $\mu_{D,bulk}$ . We observe the minimum in formation energies of substitution defects at N positions at  $\mu_N = -8.09$  eV for all defects. This indicates energetic favorability to substitute N at the N1 and N2 sites even over substitution of Zn at this special point. We speculate that the easy formation of native defect N1 vacancy (based on data from Table 3 and Fig. 3) could be another reason of this occurrence, besides the change of the  $\mu_{D,Max}$ .

For interstitial ( $I_D$ ) at high symmetry Wickoff position  $8a$  (0, 0, 0), the formation energies are calculated from Eq. (2) and listed in Table 4. They increase with the atomic radii for defects in both N-poor and N-rich conditions. The same trend is also observed at for the defect substitution at the Zn site but not at the N positions. We observe in Table 4 that the formation energies of defects of a given element follow in descending order for the defects  $D_{N2}$ ,  $D_{N1}$ ,  $I_D$ , and  $D_{Zn}$ .

### 3.4. Electronic structure

#### 3.4.1. Native defects

In Fig. 6, the DOS of pure  $Zn_3N_2$  and with different types of native defects is shown, and they correlate well with their respective formation energies in N-poor condition. With respect to its own Fermi energy, the filled and empty DOS of  $V_{N1}$  are shifted to a lower energy level, compared to the case of pure zinc nitride. A similar shift, though lesser in magnitude, is seen for the case of  $V_{N2}$  and  $I_{Zn}$ . This correlates well with these three defects exhibiting the lowest formation energies. This case contrasts with the case of  $V_{Zn}$  and  $I_N$  where the filled state DOS shifts to the right in Fig. 6 and these two defects have the highest formation energies. The shift of the DOS to a lower energy level for  $V_{N1}$ ,  $V_{N2}$ , and  $I_{Zn}$  is accompanied by the first peak in the CB getting closer to the Fermi energy ( $E_F$ ) indicative of n-type character as seen in experiment [3,6,11,18,58–60].

#### 3.4.2. Impurities — Cu family elements

Fig. 7 shows the LDOS of pure  $Zn_3N_2$  and with different substitution defects at the N1 position. The effects, in the LDOS, of substitution defects at the N2 positions are similar to those at N1. Therefore, only the N1 case is shown in Fig. 7. The LDOS is only the portion of total density of states projected onto the defect and its nearest neighbor atoms. For a substitution defect at N1 or N2 position, there are six Zn nearest neighbors. Fig. 7 shows that the magnitude of the defect-introduced states in  $Cu_{N1}$  is higher than that in  $Ag_{N1}$  or  $Au_{N1}$ . In addition, the location of these states in  $Cu_{N1}$  is different than that in  $Ag_{N1}$ , or  $Au_{N1}$ . The defect-introduced states for  $Cu_{N1}$  are located close to the top of the valence band, while in  $Ag_{N1}$  or  $Au_{N1}$ , they are located relatively higher in energy. This suggests that Cu-doped zinc nitride is likely to show p-type character while Ag- or Au-doped zinc nitride may display n-type conducting behavior.

In Fig. 8, LDOS of pure  $Zn_3N_2$  and of different substitution defects at the Zn position are presented. To differentiate the effect of first forming a vacancy by removing a Zn atom and subsequent filling of this vacancy by a dopant atom the LDOS for  $V_{Zn}$  is shown. For a substitutional defect at a Zn position, there are four N nearest neighbors. The effect of copper family elements as substitution defects at Zn position on the electronic properties at the edges of valence band and conduction band is very similar and all show an increase in the density at  $E_F$ .

Fig. 9 depicts the LDOS of pure  $Zn_3N_2$  and of different interstitial defects. To compare with native defects, LDOS for  $I_N$  and  $I_{Zn}$  are shown. The nearest neighbor atoms of the interstitial defect include six Zn atoms and six N atoms. In Fig. 9, it can be seen that the copper family elements as interstitial defects all produce a shift in the LDOS to lower energy levels. This shift is similar to the one caused by Zn as an interstitial defect.

## 4. Conclusion

Structural, electronic and energetic properties of (i) pure  $Zn_3N_2$  and (ii) point defects of native species Zn and N and copper group elements Cu, Ag and Au were investigated, with density functional theory computations. The lattice constant, bulk modulus and electronic band structure of pure  $Zn_3N_2$  were computed. The analysis of the DOS of pure  $Zn_3N_2$  showed clearly that electronic behavior is closely related to and, therefore, easily affected by nitrogen. The formation energies of both native defects and copper family element impurities are affected significantly by change of chemical potential of different species. For native defects, in N-poor condition, nitrogen vacancies and zinc interstitials are energetically favored over nitrogen interstitials. There exists a special region in parameter space, near  $\mu_N = -8.09$  eV, where substitution of N atoms, by Cu, Ag and Au, is favored over substitution of Zn atoms. The LDOS of copper family elements suggests that Cu-doped zinc nitride will tend to show the p-type character while Ag- or Au-doped zinc nitride may display n-type conducting behavior.

## Acknowledgments

The authors would like to thank the Ohio Supercomputer Center (OSC) and the National Science Foundation (NSF), through grant CNS 0855134, for providing computing resources. We thank the Wright Center for PVIC of the State of Ohio and the University of Toledo as well as the NSF (grants: CMMI 1234777, CMMI 0928440, and CMMI 0933069) for funding this work.

## References

- [1] K. Kuriyama, Y. Takahashi, F. Sunohara, Optical band gap of  $Zn_3N_2$  films, *Phys. Rev. B* 48 (1993) 2781.
- [2] D. Wang, Y.C. Liu, R. Mu, J.Y. Zhang, Y.M. Lu, D.Z. Shen, X.W. Fan, The photoluminescence properties of  $ZnO:N$  films fabricated by thermally oxidizing  $Zn_3N_2$  films using plasma-assisted metal-organic chemical vapour deposition, *J. Phys. Condens. Matter* 16 (2004) 4635.
- [3] V. Kambalafka, P. Voulgaropoulou, S. Dounis, E. Iliopoulos, M. Androulidaki, K. Tsagaraki, V. Šály, M. Ružinský, P. Prokein, E. Aperathitis, The effect of nitrogen on

- the properties of zinc nitride thin films and their conversion into p-ZnO:N films, *Thin Solid Films* 515 (2007) 8573.
- [4] C. Garcia Nunez, J.L. Pau, E. Ruiz, J. Piqueras, Thin film transistors based on zinc nitride as a channel layer for optoelectronic devices, *Appl. Phys. Lett.* 101 (2012) 253501.
- [5] N. Jiang, D.G. Georgiev, T. Wen, A.H. Jayatissa, Reactive radio frequency sputtering deposition and characterization of zinc nitride and oxynitride thin films, *Thin Solid Films* 520 (2012) 1698.
- [6] N. Jiang, D.G. Georgiev, A.H. Jayatissa, R.W. Collins, J. Chen, E. McCullen, Zinc nitride films prepared by reactive RF magnetron sputtering of zinc in nitrogen containing atmosphere, *J. Phys. D: Appl. Phys.* 45 (2012) 135101.
- [7] N. Jiang, D.G. Georgiev, A.H. Jayatissa, The effects of the pressure and the oxygen content of the sputtering gas on the structure and the properties of zinc oxynitride thin films deposited by reactive sputtering of zinc, *Semicond. Sci. Technol.* 28 (2013) 025009.
- [8] R. Juza, H. Hahn, Über die kristallstrukturen von  $Zn_3N_2$ ,  $Cd_3N_2$  und  $Ge_3N_4$ , metallamide und metallnitride. IX. mitteilung, *Z. Anorg. Allg. Chem.* 244 (1940) 125.
- [9] D.E. Partin, D.J. Williams, M. O'Keefe, The Crystal Structures of  $Mg_3N_2$  and  $Zn_3N_2$ , *J. Solid State Chem.* 132 (1997) 56.
- [10] M. Futsuhara, K. Yoshioka, O. Takai, Structural, electrical and optical properties of zinc nitride thin films prepared by reactive rf magnetron sputtering, *Thin Solid Films* 322 (1998) 274.
- [11] V. Kambalifka, P. Voulgaropoulou, S. Dounis, E. Iliopoulos, M. Androulidaki, V. Saly, M. Ruzinsky, E. Aperathitis, Thermal oxidation of n-type ZnN films made by rf-sputtering from a zinc nitride target, and their conversion into p-type films, *Superlattice. Microst.* 42 (2007) 55.
- [12] C. Wang, Z.G. Ji, K. Liu, Y. Xiang, Z.Z. Ye, p-Type ZnO thin films prepared by oxidation of  $Zn_3N_2$  thin films deposited by DC magnetron sputtering, *J. Cryst. Growth* 259 (2003) 279.
- [13] K. Toyoura, H. Tsujimura, T. Goto, K. Hachiya, R. Hagiwara, Y. Ito, Optical properties of zinc nitride formed by molten salt electrochemical process, *Thin Solid Films* 492 (2005) 88.
- [14] R. Ayouchi, C. Casteleiro, L. Santos, R. Schwarz, RF-plasma assisted PLD growth of  $Zn_3N_2$  thin films, *Phys. Status Solidi C* 7 (2010) 2294.
- [15] R. Long, Y. Dai, L. Yu, M. Guo, B.B. Huang, Structural, electronic, and optical properties of oxygen defects in  $Zn_3N_2$ , *J. Phys. Chem. B* 111 (2007) 3379.
- [16] R. Long, Y. Dai, L. Yu, B.B. Huang, S.H. Han, Atomic geometry and electronic structure of defects in  $Zn_3N_2$ , *Thin Solid Films* 516 (2008) 1297.
- [17] Z. Li, P. Wang, H.H. Chen, X.L. Cheng, Structural, electronic and thermodynamic properties of cubic  $Zn_3N_2$  under high pressure from first-principles calculations, *Physica B* 406 (2011) 1182.
- [18] T. Suda, K. Kakishita, Band-gap energy and electron effective mass of polycrystalline  $Zn_3N_2$ , *J. Appl. Phys.* 99 (2006) 076101.
- [19] F.J. Zong, H.L. Ma, W. Du, X.J. Zhang, H.D. Xiao, F. Ji, Structural properties and photoluminescence of zinc nitride nanowires, *Appl. Phys. Lett.* 87 (2005) 233104.
- [20] Y. Yan, M.M. Al-Jassim, S.H. Wei, Doping of ZnO by group-IB elements, *Appl. Phys. Lett.* 89 (2006) 181912.
- [21] P. Hohenberg, W. Kohn, Inhomogeneous Electron Gas, *Phys. Rev. B* 136 (1964) B864.
- [22] W. Kohn, L.J. Sham, Self-consistent equations including exchange and correlation effects, *Phys. Rev.* 140 (1965) A1133.
- [23] G. Kresse, J. Hafner, Ab initio molecular dynamics for liquid metals, *Phys. Rev. B* 47 (1993) 558.
- [24] G. Kresse, Ab initio molekular dynamik für flüssige metalle, (Ph.D thesis) Technische Universität Wien, Austria, 1993.
- [25] G. Kresse, J. Furthmüller, Efficiency of ab-initio total energy calculations for metals and semiconductors using a plane-wave basis set, *Comput. Mater. Sci.* 6 (1996) 15.
- [26] G. Kresse, J. Furthmüller, Efficient iterative schemes for ab initio total-energy calculations using a plane-wave basis set, *Phys. Rev. B* 54 (1996) 11169.
- [27] D. Vanderbilt, Soft self-consistent pseudopotentials in a generalized eigenvalue formalism, *Phys. Rev. B* 41 (1990) 7892.
- [28] G. Kresse, J. Hafner, Norm-conserving and ultrasoft pseudopotentials for first-row and transition elements, *J. Phys. Condens. Matter* 6 (1994) 8245.
- [29] J.P. Perdew, A. Zunger, Self-interaction correction to density-functional approximations for many-electron systems, *Phys. Rev. B* 23 (1981) 5048.
- [30] J.P. Perdew, J.A. Chevary, S.H. Vosko, K.A. Jackson, M.R. Pederson, D.J. Singh, C. Fiolhais, Atoms, molecules, solids, and surfaces: Applications of the generalized gradient approximation for exchange and correlation, *Phys. Rev. B* 46 (1992) 6671.
- [31] J.P. Perdew, J.A. Chevary, S.H. Vosko, K.A. Jackson, M.R. Pederson, D.J. Singh, C. Fiolhais, Erratum: Atoms, molecules, solids, and surfaces: Applications of the generalized gradient approximation for exchange and correlation, *Phys. Rev. B* 48 (1993) 4978.
- [32] H.J. Monkhorst, J.D. Pack, Special points for Brillouin-zone integrations, *Phys. Rev. B* 13 (1976) 5188.
- [33] M. Methfessel, A.T. Paxton, High-precision sampling for Brillouin-zone integration in metals, *Phys. Rev. B* 40 (1989) 3616.
- [34] T. Hahn (Ed.), 2002 International Tables for Crystallography Volume A: Space-Group Symmetry, 5th ed., Springer, Netherlands, 2002, p. 663.
- [35] S.K.R. Patil, N.S. Mangale, S.V. Khare, S. Marsillac, Super hard cubic phases of period VI transition metal nitrides: First principles investigation, *Thin Solid Films* 517 (2008) 824.
- [36] S. Kodambaka, S.V. Khare, V. Petrova, D.D. Johnson, I. Petrov, J.E. Greene, Absolute orientation-dependent anisotropic TiN(111) island step energies and stiffnesses from shape fluctuation analyses, *Phys. Rev. B* 67 (2003) 35409.
- [37] H.A. Mohamed, Structure and optical constants of electron beam deposited zinc nitride films, *Eur. Phys. J. Appl. Phys.* 48 (2009) 20504.
- [38] J.G. Zhao, L.X. Yang, S.J. You, F.Y. Li, C.Q. Jin, J. Liu, Structural stability of  $Zn_3N_2$  under high pressure, *Physica B* 405 (2010) 1836.
- [39] S.H. Wei, S.B. Zhang, Chemical trends of defect formation and doping limit in II-VI semiconductors: The case of CdTe, *Phys. Rev. B* 66 (2002) 155211.
- [40] S.B. Zhang, J.E. Northrup, Chemical potential dependence of defect formation energies in GaAs: Application to Ga self-diffusion, *Phys. Rev. Lett.* 67 (1991) 2339.
- [41] C.G. Van de Walle, J. Neugebauer, Atomic geometry and electronic structure of native defects in GaN, *Phys. Rev. B* 50 (1994) 8067.
- [42] C.G. Van de Walle, S. Limpijumnong, First-principles studies of beryllium doping of GaN, *Phys. Rev. B* 63 (2001) 245205.
- [43] C.G. Van de Walle, J. Neugebauer, First-principles calculations for defects and impurities: Applications to III-nitrides, *J. Appl. Phys.* 95 (2004) 3851.
- [44] R. Ramprasad, H. Zhu, P. Rinke, M. Scheffler, New perspective on formation energies and energy levels of point defects in nonmetals, *Phys. Rev. Lett.* 108 (2012) 066404.
- [45] D.B. Laks, C.G. Van de Walle, G.F. Neumark, P.E. Blochl, S.T. Pantelides, Native defects and self-compensation in ZnSe, *Phys. Rev. B* 45 (1992) 10965.
- [46] G.A. Baraff, M. Schluter, Electronic Structure, Total Energies, and Abundances of the Elementary Point Defects in GaAs, *Phys. Rev. Lett.* 55 (1985) 1327.
- [47] T.B. Massalski, U. Mizutani, Electronic structure of Hume-Rothery phases, *Prog. Mater. Sci.* 22 (1978) 151.
- [48] K.W. Andrews, H.E. Davies, W. Hume-Rothery, C.R. Oswin, The equilibrium diagram of the system silver-zinc, *Proc. R. Soc. Lond. A* 177 (1941) 149.
- [49] H.S. Liu, K. Ishida, Z.P. Jin, Y. Du, Thermodynamic assessment of the Au-Zn binary system, *Intermetallics* 11 (2003) 987.
- [50] T. Mattila, R.M. Nieminen, Ab initio study of oxygen point defects in GaAs, GaN, and AlN, *Phys. Rev. B* 54 (1996) 16676.
- [51] A. Soon, L. Wong, M. Lee, M. Todorova, B. Delley, C. Stampfl, Nitrogen adsorption and thin surface nitrides on Cu(111) from first-principles, *Surf. Sci.* 601 (2007) 4775.
- [52] N. Greenwood, A. Earnshaw, Chemistry of the Elements, Butterworth-Heinemann, UK, 1997.
- [53] E. Gregoryanz, C. Sanloup, M. Somayazulu, J. Badro, G. Fiquet, H. Mao, R.J. Hemley, Synthesis and characterization of a binary noble metal nitride, *Nat. Mater.* 3 (2004) 294.
- [54] S.K.R. Patil, S.V. Khare, B.R. Tuttle, J.K. Bording, S. Kodambaka, Mechanical stability of possible structures of PtN investigated using first-principles calculations, *Phys. Rev. B* 73 (2006) 104118.
- [55] J.C. Crowhurst, A.F. Goncharov, B. Sadigh, C.L. Evans, P.G. Morrall, J.L. Ferreira, A.J. Nelson, Synthesis and characterization of the nitrides of platinum and iridium, *Science* 311 (2006) 1275.
- [56] F. Fischer, A. Waag, G. Bilger, T. Litz, S. Scholl, M. Schmitt, G. Landwehr, Molecular beam epitaxy of iodine-doped CdTe and (CdMg)Te, *J. Cryst. Growth* 141 (1994) 93.
- [57] C.S. Ferekides, V. Viswanathan, D.L. Morel, RF sputtered back contacts for CdTe/CdS thin film solar cells, Proceeding of IEEE Photovoltaic Specialists Conference, 1997, p. 423.
- [58] G.Z. Xing, D.D. Wang, B. Yao, L.F.N. Ah. Qune, T. Yang, Q. He, J.H. Yang, L.L. Yang, Structural and electrical characteristics of high quality (100) orientated- $Zn_3N_2$  thin films grown by radio-frequency magnetron sputtering, *J. Appl. Phys.* 108 (2010) 083710.
- [59] P. Voulgaropoulou, S. Dounis, V. Kambalifka, M. Androulidaki, M. Ruzinsky, V. Saly, P. Prokein, Z. Viskadourakis, K. Tsagaraki, E. Aperathitis, Optical properties of zinc nitride thin films fabricated by rf-sputtering from ZnN target, *Thin Solid Films* 516 (2008) 8170.
- [60] N. Jiang, D.G. Georgiev, A.H. Jayatissa, T. Wen, Zinc nitride films by reactive sputtering of Zn in  $N_2$ -containing atmosphere, *Mater. Res. Soc. Symp. Proc.* 1324 (2011) 157.